International Journal of Thermophysics (2022) 43:36
https://doi.org/10.1007/s10765-021-02963-1

Imaging Luminescence Thermometry to 750 °C for the Heat Treatment of Common Engineering Alloys and Comparison with Thermal Imaging

Gavin Sutton[1] · Sofia Korniliou[1] · Aurik Andreu[2] · David Wilson[2]

Received: 8 November 2021 / Accepted: 8 December 2021 / Published online: 10 January 2022

Abstract

Accurate temperature measurements are critical in manufacturing, affecting both product quality and energy consumption. At elevated temperatures, non-contact thermometers are often the only option. However, such instruments require prior knowledge of the surface emissivity, which is often unknown or difficult to determine, leading to large errors. Here we present a novel imaging luminescence thermometer based on the intensity ratio technique using magnesium fluorogermanate phosphor, with the potential to overcome this limitation. We describe measurements performed on a number of engineering alloys undergoing heat treatment at temperatures of up to 750 °C and compare these measurements against a traditional contact thermocouple and thermal imager system. Agreement between the luminescence and embedded thermocouple temperatures was found to be better than 45 °C at all temperatures. However, the thermal imager measurement on the bare metal samples, with the instrument emissivity set to 1.0, showed differences of up to 500 °C at 750 °C, a factor of 10 larger. In an effort to improve the thermal imager accuracy, its instrument emissivity was adjusted until its temperature agreed with that of the thermocouple. When measuring on the bare metal, the effective emissivity was strongly sample dependent, with mean values ranging from 0.205 to 0.784. Since the phosphor derived temperatures exhibited substantially smaller errors compared to the thermal imager, it is suggested that this method can be used to compliment the thermal imaging technique, by providing a robust mechanism for adjustment of the instrument emissivity until agreement between the thermal imager and phosphor thermometer is obtained.

Keywords Heat treatment · Imaging · Luminescence · Phosphor · Thermometry

✉ Gavin Sutton
gavin.sutton@npl.co.uk

[1] Thermal and Radiometric Metrology, National Physical Laboratory, Teddington, UK

[2] Advanced Forming Research Centre, University of Strathclyde, Glasgow, UK

1 Introduction

Accurate, traceable temperature measurements are critical in many high value manufacturing applications, particularly at elevated temperatures [1–3]. For example, successful thermal processing of metals during forging and forming processes is critically dependent on process temperature [4]. Traditionally, surface temperatures are determined by infrared thermometry (spot pyrometers or thermal images) or sprung-loaded thermocouples. However, it is known that these approaches can have large uncertainties, due to unknown emissivity and background radiation in the former case [5–7] and due to variable contact and heat-sink effects in the latter case [8]. Luminescence thermometry, where a coating applied to the surface is interrogated optically, has the potential to overcome these limitations [9] and, when correctly applied is independent of the surface emissivity and unperturbed by strong background thermal radiation.

Here, we describe an imaging luminescence thermometry system developed during the Euramet EMPIR project EMPRESS 2 [2] capable of remotely measuring surface temperatures of up to 750 °C with low uncertainty. Imaging technologies offer many advantages over single point measurements, primarily in their capability to map an entire surface and the ability to spatially resolve temperature gradients. However, we concentrate here on the comparison of phosphor thermometry with thermal imaging over a small, localised region during the heat treatment of typical engineering alloys and demonstrate how it is possible to improve on/compliment the well-established thermal imaging technique.

Firstly, the basic measurement principles of the two most common methods of luminescence thermometry are described—decay time and intensity ratio—and the luminescence thermal imaging system based on the intensity ratio technique, developed at NPL, is presented in detail.

Secondly, luminescence temperature measurements on three different engineering alloy samples (nickel super alloy *Nimonic 105*, *C42 MOD steel* and *titanium Ti64*) specially prepared with a region of luminescent coating and an embedded thermocouple, heated in an induction furnace up to 750 °C are presented and compared with thermocouple and thermal imaging measurements. These measurement were performed at the Advanced Forming Research Centre, AFRC, with details of the sample preparation, the thermal imaging camera and the measurement campaign given in Sects. 3, 4 and 5, respectively.

The results of the comparison are presented in Sect. 6, where, additionally, the thermal imager instrument emissivity is determined based on the luminescence/thermocouple derived temperatures. We conclude with a summary of our findings and briefly discuss possible future work. We also include comprehensive details of the luminescence imager calibration performed at NPL prior to trials in Sect. 9—Appendix 1 and the tabulated trial results in Sect. 10—Appendix 2.

2 Luminescence Thermometry

2.1 Introduction

Thermographic phosphors exhibit a change in their temporal or spectral luminescence properties during or following excitation with UV or near-UV light. For a comprehensive summary of phosphor thermometry, we refer the reader to the review articles [9–11], with details of our earlier work given in [12]. Here we confine ourselves to the basic principles of the two most common phosphor thermometry techniques: decay time and intensity ratio.

2.2 Luminescence Decay Time Thermometry

The principle of luminescence decay time thermometry is shown in Fig. 1. The phosphor is excited with UV/blue light, and when the excitation is switched off, the luminescence intensity decays exponentially. In this example for Manganese doped magnesium fluorogermanate phosphor (MFG), the emission is in a band around 660 nm (red light). The decay time, τ, is determined by fitting a single exponential function $I(t) = A + Be^{-it/\tau}$ to the decay signal. The decay time decreases monotonically with increasing temperature T, and through suitable calibration, the relationship between τ and T can be established (see insert in Fig. 1). Following calibration, subsequent measurements of τ allow the temperature to be determined uniquely.

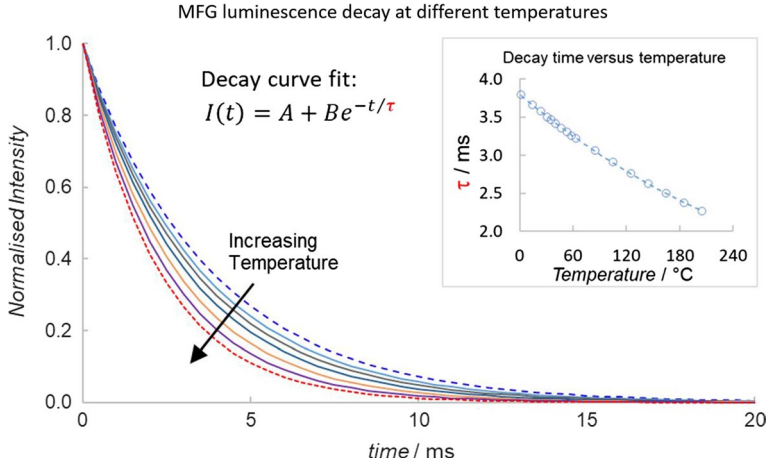

Fig. 1 Principle of decay time luminescence thermometry: the decay time, τ, reduces monotonically with increasing temperature (see insert). The example shown here is for the phosphor MFG

2.3 Luminescence Intensity Ratio Thermometry

The principle of luminescence intensity ratio thermometry is shown in Fig. 2. The phosphor is excited continuously with UV/blue light, and the luminescence intensity measured simultaneously in two narrow wavelength bands. In this example (for MFG), the emission peaks at 635 nm and 660 nm are used, with the former increasing and the latter decreasing in intensity, respectively, with increasing temperature. The intensity ratio, $\phi = I(635\text{nm})/I(660\text{nm})$, versus temperature is then established through suitable calibration (see inset in Fig. 2). Following calibration, subsequent measurements of ϕ allow the temperature to be determined uniquely.

2.4 Imaging Luminescence Thermometry

Imaging luminescence thermometry can be implemented for both decay time and intensity ratio techniques. In our previous work [12] we presented an imaging system based on the decay time method, where three images are captured with a single camera at different times after extinction of the excitation light: 1) immediately following extinction, 2) a fixed time after extinction and 3) once all luminescence has ceased (background measurement). We refer the reader to the publication for full details. The weakness of the decay time technique, when used with MFG phosphor, was an upper temperature limit of 450 °C, primarily due to the lack of luminescence in the second captured image.

In this work, we decided to build on our experience with MFG, but move to a camera system based on the intensity ratio technique. The benefit of doing this is that the luminescence images can be collected while the phosphor is illuminated, resulting in significantly larger signals and an extension of the upper temperature limit to 750 °C.

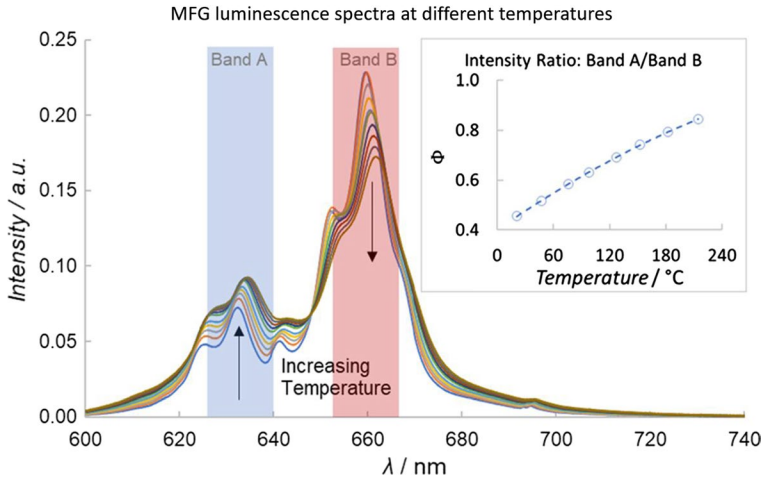

Fig. 2 Principle of intensity ratio luminescence thermometry: the intensity ratio ϕ, increases monotonically with increasing temperature (see insert). The example shown here is for the phosphor MFG

The imaging intensity ratio system comprises two components—a robust thermographic phosphor coating, and a camera system with bespoke measurement software. The coating was prepared by Indestructible Paints (IP) [13] using manganese doped magnesium fluorogermanate (Mg_4FGeO_6:Mn) thermographic phosphor (MFG), provided by OSRAM [14].

2.5 Coating Preparation

The coating comprised a mixture of proprietary resin (40.49%), MFG powder (39.27%) and solvent (20.24%). The components were added to a stainless steel pot along with glass beads as a grinding media. The mixture was placed on a high shear dispersing blade and blended until a Hegman Grind of < 10 µm was reached, and the glass beads were filtered out once the grind was achieved. The substrate was prepared by cleaning with solvent degrease followed by a light grit blast with 150 mesh grit. The mixture was applied to the substrate using a gravity-fed air assisted spray gun, and the coating was left to dry in air for 15 min then a further 30 min at 100 °C.

2.6 The Camera System

The system operates in the intensity ratio mode, where two luminescence images captured consecutively at 635 nm and 660 nm are ratioed pixel-by-pixel to generate an intensity ratio map. The relationship between the intensity ratio and temperature is found by calibration and is described in the Appendix 1. The instrument comprises:

(1) Thorlabs [15] CS505MU CMOS 5 MP monochrome scientific camera with external trigger
(2) Nikon 60 mm F/2.8 lens
(3) Thorlabs motorised filter flipper mount MFF101/M
(4) Prizmatix [16] UHP-T-405-DI high-power LED (405 nm, 5 W) and driver, and lens arrangement.
(5) Two bandpass interference filters (10 nm FWHM)—$\lambda_1 = 635$ nm (FLH635-10) and $\lambda_2 = 660$ nm (FBH660-10). The two bandpass filters were installed in the flipper mount
(6) National Instruments (NI) [17] USB DAQ system to provide triggers for the flipper/LED/ camera
(7) NI LabView software to control the instrument and collect measurements

The luminescence thermometer set-up is shown in Fig. 3a), where the filter flipper is used to select the measurement wavelength by moving one of two filters in front of the camera. The principle of operation is shown in Fig. 3b), where each cycle takes four seconds: *Flipper*—a positive or negative voltage causes the flipper to move to position 1 ($\lambda = 635$ nm) or position 2 ($\lambda = 660$ nm) respectively; *LED*—the magnitude and timing of the excitation source (LED); *Cam trig*—camera images are captured on a rising edge; *Cam exp*—the camera exposure (time).

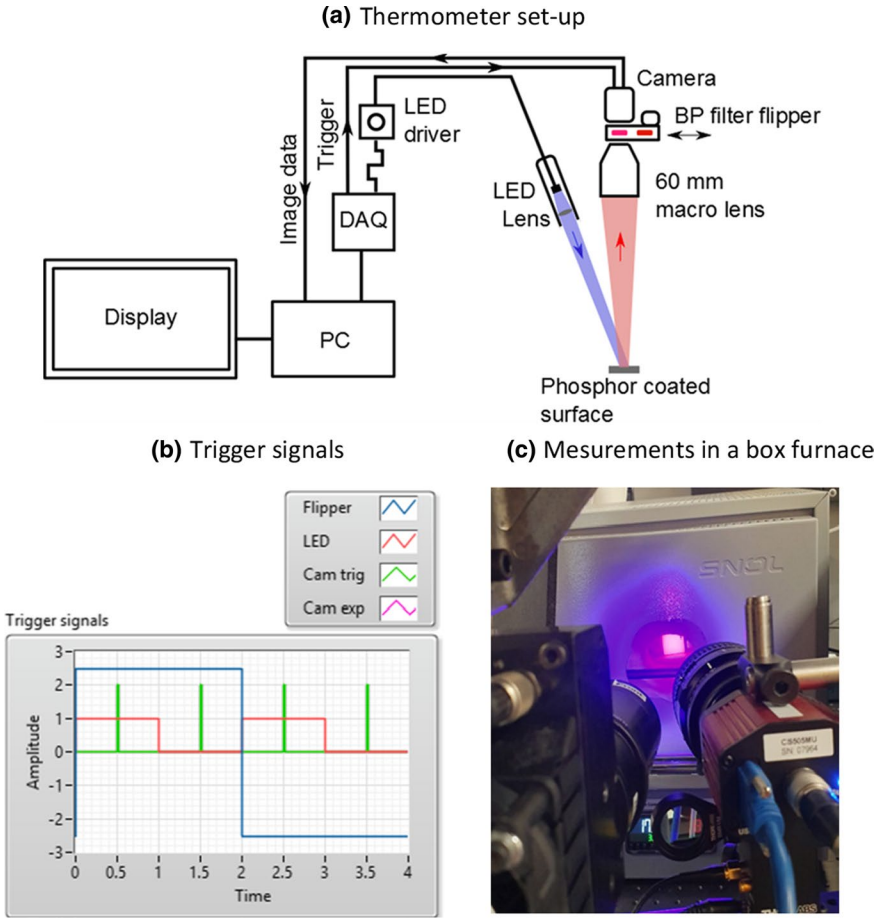

Fig. 3 The imaging intensity ratio luminescence thermometer: (a) set-up, (b) trigger signals and (c) measurement example—phosphor coated sample during measurement through a sapphire window in the small box furnace

For each measurement cycle, four images are captured, two at each wavelength. At each wavelength, images are captured during steady-state phosphor luminescence (emission) and a fixed time after emission has ceased (background), with the background image subtracted from the emission. Figure 3c) shows the phosphor thermometer measuring a sample within a box furnace through a large sapphire window. A 2D temperature map is obtained for each measurement cycle, which takes 4 s.

The bespoke software is used to perform all measurements. The temperature maps are determined as follows:

1. The four images are captured, two at each wavelength, for emission and background:

$$\begin{aligned} &I_{1,1}(x_i, y_j) \quad \text{emission atl} = 635\text{nm} \\ &I_{2,1}(x_i, y_j) \quad \text{emission atl} = 660\text{nm} \\ &I_{1,0}(x_i, y_j) \quad \text{background atl} = 635\text{nm} \\ &I_{2,0}(x_i, y_j) \quad \text{background atl} = 660\text{nm} \end{aligned} \tag{1}$$

The background images are subtracted pixel-by-pixel from the emission images:

$$\begin{aligned} I_1(x_i, y_j) &= I_{1,1}(x_i, y_j) - I_{1,0}(x_i, y_j) \\ I_2(x_i, y_j) &= I_{2,1}(x_i, y_j) - I_{2,0}(x_i, y_j) \end{aligned} \tag{2}$$

2. The resulting 660 nm image $I_2(x_i, y_j)$ is adjusted in software so that each pixel measured at 635 nm is aligned with that at 660 nm. This is required because of differences in the position of the image on the camera sensor introduced by each filter. This alignment offset is determined prior to measurements by calculating the 2D cross correlation of an image captured at each wavelength. For these measurements, the offset between images at 635 nm and 660 nm was $(\Delta x, \Delta y) = (2, -3)$ pixels, and aligning the images significantly reduced the apparent noise in the measured intensity ratio and thus temperature:

$$\begin{aligned} I_1^{\mathrm{A}}(x_i, y_j) &= I_1(x_i, y_j) \\ I_2^{\mathrm{A}}(x_i, y_j) &= I_2(x_i + \Delta x, y_j + \Delta y) \end{aligned} \tag{3}$$

3. The images are then binned $\times 8$ times in software, i.e. the values of each 8×8 pixel cluster are averaged. This results in an image with a resolution of 306×256 pixels and reduces the full sensor resolution of 2448×2048 pixels by a factor of 8, but also reduces the standard deviation of the measurements by the same factor:

$$\begin{aligned} I_1^{A}(x_i, y_j) &\rightarrow I_1^{\mathrm{AB}}(x_i, y_j) \\ I_2^{\mathrm{A}}(x_i, y_j) &\rightarrow I_2^{\mathrm{AB}}(x_i, y_j) \end{aligned} \tag{4}$$

4. A second algorithm, we call *Joggle*, is applied to the images that performs the equivalent of a Gaussian blur to each image. This further reduces the apparent noise on the images:

$$\begin{aligned} I_1^{\mathrm{AB}}(x_i, y_j) &\rightarrow I_1^{\mathrm{ABJ}}(x_i, y_j) \\ I_2^{\mathrm{AB}}(x_i, y_j) &\rightarrow I_2^{\mathrm{ABJ}}(x_i, y_j) \end{aligned} \tag{5}$$

5. The intensity ratio image is now determined by dividing, pixel-by-pixel, the two resultant images:

$$IR(x_i, y_j) = \frac{I_1^{\mathrm{ABJ}}(x_i, y_j)}{I_2^{\mathrm{ABJ}}(x_i, y_j)} \tag{6}$$

6. To convert the intensity ratio (*IR*) image to a temperature (*T*) image, a calibration file of *T* versus *IR*, captured previously is used. For each pixel in the *IR* image, the associated *T* is found in the calibration file through interpolation:

$$T(x_i, y_j) = \mathrm{Fn}\left[IR(x_i, y_j), T_{\mathrm{cal}}, IR_{\mathrm{cal}}\right] \tag{7}$$

7. Using this level of binning, image realignment and *joggle*, the standard deviation of each pixel is typically less than 1 °C at room temperature.

3 Thermal Imager

The thermal imager used in this work was a LAND ARC-8–22-1000-HF [18], with a measurement temperature range from 100 °C to 1000 °C, an operating wavelength of 8 µm–14 µm, and a field of view of 22°. It has an adjustable focal range, controlled remotely in software, from 0.3 m to infinity. This camera provides a framerate of 30 fps, at a fixed resolution of 384 pixels x 288 pixels. The manufacturers claim an accuracy of ± 2% or ± 2 °C. The emissivity as well a background temperature correction can be adjusted in software. The imager was calibrated (with the instrument emissivity setting equal to 1.00) by the supplier, prior to tests, against traceable blackbody standards, with an uncertainty of 5.0 °C or less over the temperature range from 100 to 700 °C [19].

4 Sample Preparation

The AFRC provided seven metal samples to prepare for testing. Each sample was machined into a 20 × 20 × 45 mm block, with a 2 mm diameter hole in the rear, drilled to a depth of 2 mm below the front surface. These are shown in Fig. 4a) as supplied, b) following machining, and c) following a single heat-up cycle (700 °C) in an argon purged furnace—some oxidation is evident. Sample 5 was used for phosphor calibration and sample 6 has not been heated at this point. Following machining, the samples were sent to IP for the phosphor coating to be applied to half of the front surface—see Fig. 4c). The coating thickness, measured with a *Sauter TC 1250–0.1 F* Thickness Gauge [20] was found to be between 60 µm and 100 µm for all samples.

5 Measurements

Three of the seven samples described in Sect. 4 were tested in field trials at the AFRC: 1) Sample 3—*Nimonic 105*, 2) Sample 2—*C42 MOD steel*, and 3) Sample 6—*Ti64*. As described earlier, the front surface of each sample is covered on one half (1 cm x 2 cm) with the IP/MFG coating, the other half being uncoated bare metal. In turn, each sample was mounted on a refractory support in the centre of the inductor of an induction furnace for heat treatment. A traceable, Type-N,

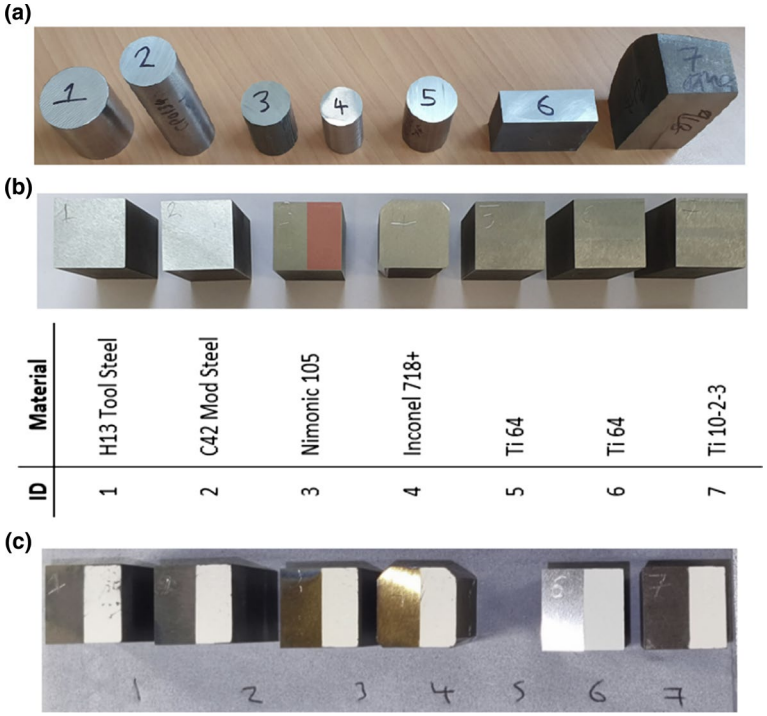

Fig. 4 Preparation of metal alloy samples for AFCR trials: a) as supplied, b) following machining—Sample 3 shows an indication of where the phosphor coating will be applied, and c) following coating application and a single heat-up cycle (700 °C)—apart from sample 6, which has not been heat cycled and remains as machined. Sample 5 is not shown as it was used for phosphor calibration purposes

1 mm diameter (mineral insulated, stainless steel sheathed) thermocouple was placed in a hole from the rear of the samples with the tip 2 mm behind the middle of the front surface.

The furnace was a 15 kW Ambrell Ekoheat induction heating system in conjunction with a large inductor. The inductor and electronics were water cooled using a recirculating chiller. The copper coil had a wall thickness of 0.81 mm, an internal diameter of 97 mm and was mounted within a refractory concrete enclosure with an empty tubular region of ID 87 mm in its centre for sample placement. The coil had 6 turns with a working length of 95 mm. The settings for the induction heating control system were as follow:

- Resonant frequency: 92 kHz to 93 kHz. Tap setting: 16.
- Capacitance: series/parallel arrangement (– (2 μF × 1 μF)—(2 μF × 1 μF)—> equivalent to 1 μF).
- Starting voltage: approximately 100 V (increased up to 280 V to reach the maximum sample temperature of 700 °C). The voltage settings for each sample varied due to differences in their thermal, electrical, and magnetic properties.

- Temperature control was achieved manually by adjustment of the induction voltage and in some cases, adjustment of the power control.

The luminescence thermometer and thermal imager were placed 0.75 m away from the sample front surface, with both focused on that surface. Suitable blackout shields were placed around the system to avoid exposure to the high-power 405 nm LED. The samples were heated up to stable nominal temperatures of 200 °C–700 °C, in 100 °C steps, and stability was achieved within approximately 15 to 30 min (dependent on temperature) following a step temperature change. Figure 5 shows the measurement set-up.

At each temperature, the following measurements were made:

1. Thermocouple (T_c) temperature—2 mm below the centre of the front of the sample.
2. Thermal imager (*TI*) temperature:
    a. Temperature of the bare metal (1) and the phosphor (2), with the instrument emissivity set to $\varepsilon = 1$. See Fig. 6a).
    b. The instrument emissivity was adjusted until the *TI* temperature was equal that of the T_c for first, the bare metal, and then, the phosphor coating. The two emissivity values were recorded.
3. Phosphor temperature (mean of 4 lines/2 areas)—see Fig. 6b) for luminescence image and Fig. 6c) for the spatial temperature map and measurement regions.
4. Two repeat measurements were made for Sample 2 during cool-down.

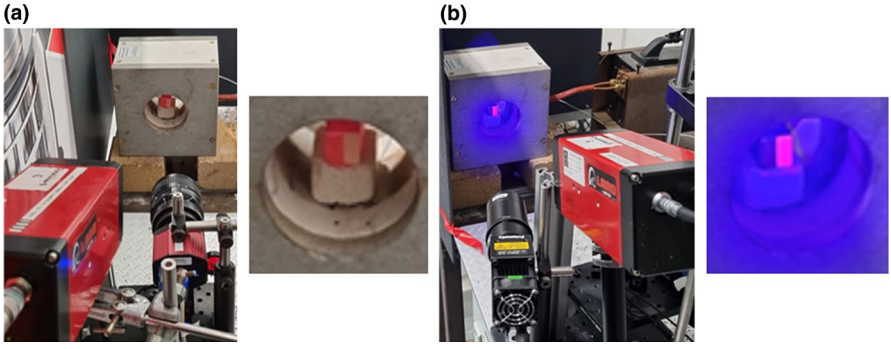

Fig. 5 Measurement set-up for the heat treatment trials: (a) no LED excitation—the thermal imager and luminescence cameras can be seen on the LHS and RHS of the left image, respectively, (b) during LED excitation—the luminescence of the phosphor coating can be seen on the surface of the sample and the excitation LED is seen on the lower LHS of the left image

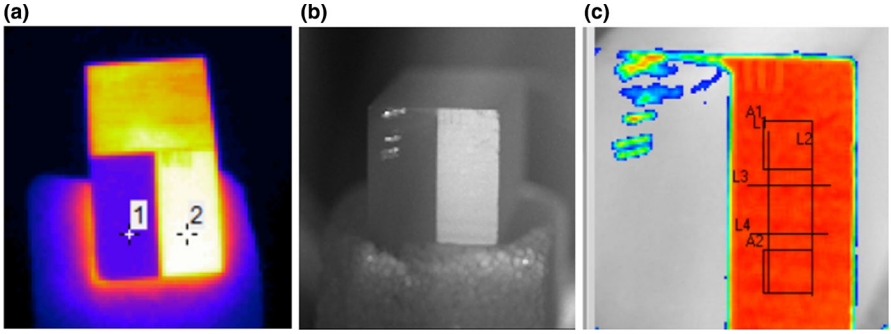

Fig. 6 Images taken from (a) the Land thermal imager—showing the measurement locations for (1) the bare metal and (2) the phosphor coating, (b) the luminescence thermometer—the raw luminescence image measured at 635 nm, and (c) the luminescence thermal image showing the measurement lines/areas extracted for later processing

6 Results

The full tabulated results can be found in Sect. 10—Appendix 2.

6.1 Luminescence Temperatures

Figure 7 shows a comparison of luminescence and thermocouple temperatures: a) absolute and b) differences. We see that the differences are less than 45 °C over the whole temperature range (200 °C to 700 °C). Three points are worthy of further discussion.

Firstly, for all three samples, above 600 °C, the phosphor thermometer measures a higher temperature than that of the thermocouple. At these temperatures, the luminescence intensity is low, and the excitation intensity of the LED needed to be substantially increased to be able to measure sufficient signals for robust determination of the intensity ratio and hence luminescence temperature. Under these conditions, and as a result of imperfect out-of-band filter blocking, it is believed that there is a contribution from the reflected excitation light (405 nm) in the measured signals at 635 nm and 660 nm. This contribution may have been different between calibration and trials due to different physical instrument configurations, for example, differences in the position of the excitation LED and camera relative to the sample. Another possibility is that differences in the heating method between calibration and trials (tube furnace versus induction furnace) may change the relationship between the thermocouple and luminescence temperatures.

Secondly, below 600 °C, the phosphor temperature is lower than that of the thermocouple in all cases. This may be explained by the fact that there will be a temperature gradient between the thermocouple, 2 mm below the surface and phosphor coating on the surface. During the calibration process, great care was taken to account for these temperature gradients (see Appendix 1). However, due to the nature of the induction heating method—heating is only generated in a thin surface layer of the metal (i.e. in those that are parallel to the induction coils

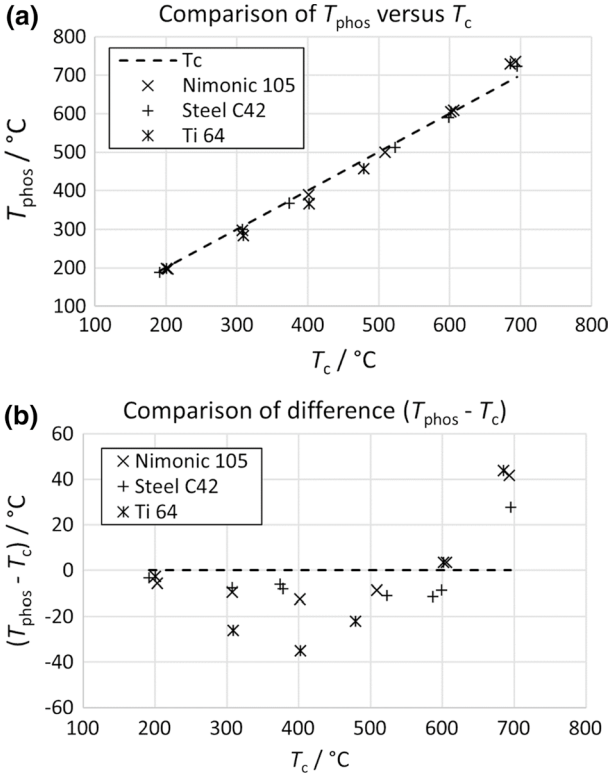

Fig. 7 Comparison of luminescence and thermocouple temperatures: (a) absolute and (b) differences

axis), it is difficult to determine what differences in temperature actually exist during trials measurements. We note that from Fig. 18, in Appendix 1, the calibration uncertainty is less than 12 °C over the full 20 °C–750 °C temperature range, so these results suggest that real temperature differences are present.

Thirdly, below 600 °C, the phosphor temperatures are significantly lower than the thermocouple temperatures for sample 6—*Ti64* (up to -35 °C), compared to samples 3—*Nimonic 105* and sample 2—*C42 MOD steel* (up to -12.4 °C). This is believed to be due to the fact that sample 6 was not pre-heated prior to trials, whereas the other two samples were pre-heated to 700 °C, resulting in annealing of the coating in the latter case and a minor change in luminescence calibration. During initial heating of sample 6—*Ti64*, the colour of the phosphor coating appeared to change from white (at room temperature) to grey (at 200 °C) and back to white (at 700 °C), supporting the hypothesis that the annealing process changes the physical appearance, at least, of the coating.

Figure 8 shows the *Ti64* sample at 200 °C on the first heat-up cycle, stopped at this temperature, and following a second heat-up cycle from room temperature to 700 °C and back to 200 °C. Between the two tests, the sample was rotated by 90° to see if the position of the phosphor relative to the supporting insulation brick

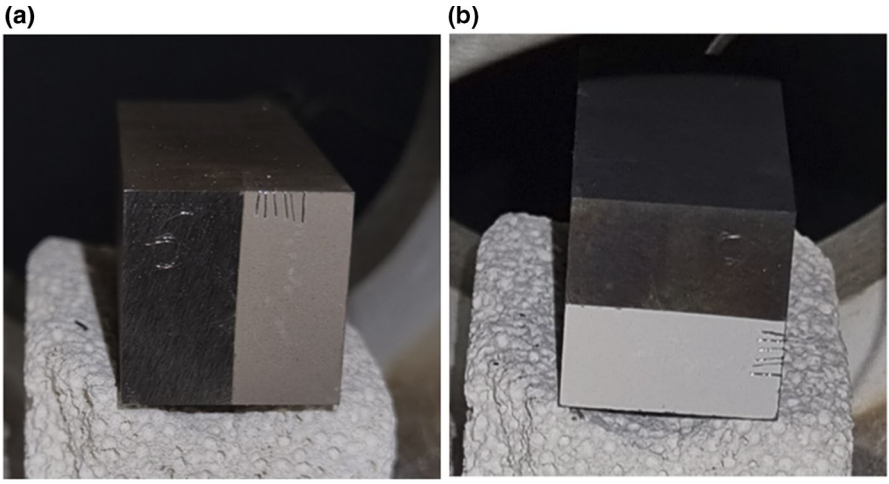

Fig. 8 Sample 6 *Ti64* during heat treatment: this was only sample not pre-heat treated. In (a) the coating appeared to turn grey as it was heated to 200 °C—there were also large differences between *T*c and *T*phos (see Fig. 7). In (b) the sample was cooled from 200 °C, rotated by 90° and re-heated—the coating appeared white once it reached 700 °C

accounted for the measured temperatures differences. The thermocouple temperatures were repeatable in the two configurations, suggesting that the bulk temperatures remained similar.

7 Thermal Imager Temperatures

Assuming that the thermocouple measurements provide a reasonable estimation of the sample surface temperature, Fig. 9 shows the temperature errors in the thermal imager measurements of a) the phosphor coating and b) the bare metal. In all cases, the thermal imager's emissivity was set to $\varepsilon = 1$.

In Fig. 9a), for measurements on the phosphor coating, we see that the errors are relatively small, increasing from -14 °C to -32 °C at 200 °C to -86 °C to -107 °C at 700 °C. In Fig. 9b), for measurements on the bare metal, we see that the errors are significantly larger, varying strongly with sample. In the absence of any prior knowledge of the surface emissivities of the bare metal surfaces, it is clear that the assumption that the surface emissivity is equal to 1 is a poor choice, leading to temperature errors at 700 °C of up to 100 °C for *C42 MOD steel*, and 431 °C and 488 °C, for *Nimonic 105* and *Ti64*, respectively.

These results and those presented in Sect. 6.1 suggest that luminescence thermometry, can be used to determine the true surface temperature and provide a mechanism to correct the thermal imager measurements. This is explored further in Sect. 6.3.

In the absence of a luminescence thermometer, it may be beneficial to simply measure the phosphor coating temperature using a thermal imager (with $\varepsilon = 1$),

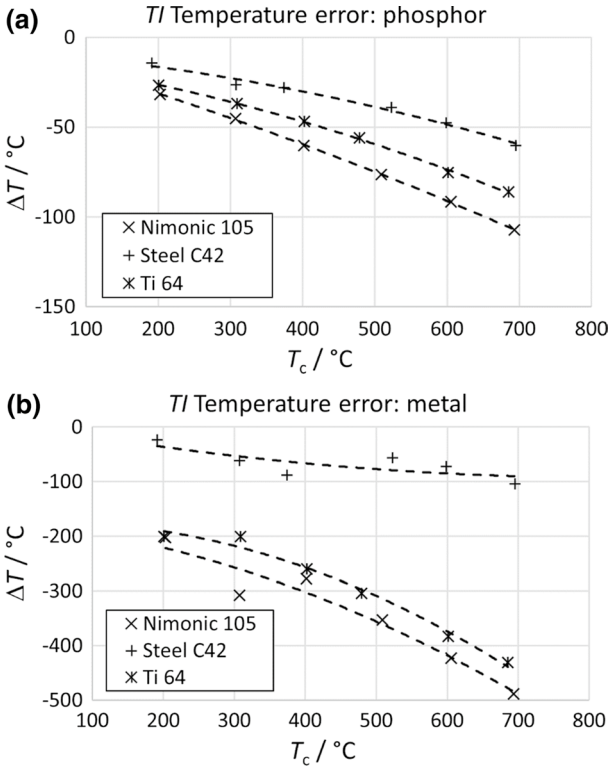

Fig. 9 Comparison of Thermal imager temperature errors when measuring on a) the phosphor coating and b) the bare metal. The instrument emissivity is set to $\varepsilon = 1$ for all measurements

where the errors due to unknown emissivity are smaller, especially for metal surfaces with a low emissivity. However, caution is advised, as the presence of the coating will perturb the energy balance of the surface and may perturb the temperature. Quantification of this effect is beyond the scope of this work but would depend on a number of factors including the sample temperature, emissivity vs wavelength/temperature relationship and the thermal properties of the coating/substrate.

8 Thermal Imager Effective Emissivities

Figure 10 shows the effective emissivities of a) the phosphor coating and b) the bare metal, for the three samples tested in the trials. This was achieved by adjusting the thermal imager's emissivity until its temperature agreed with that of the thermocouple, when measuring on first the phosphor coating and then the bare metal. In the case of the phosphor coating, we see that the effective emissivity is relatively high, ranging from 0.72 to 0.95, reducing slightly with increasing temperature. In the case of the bare metal, we see that the effective emissivity is

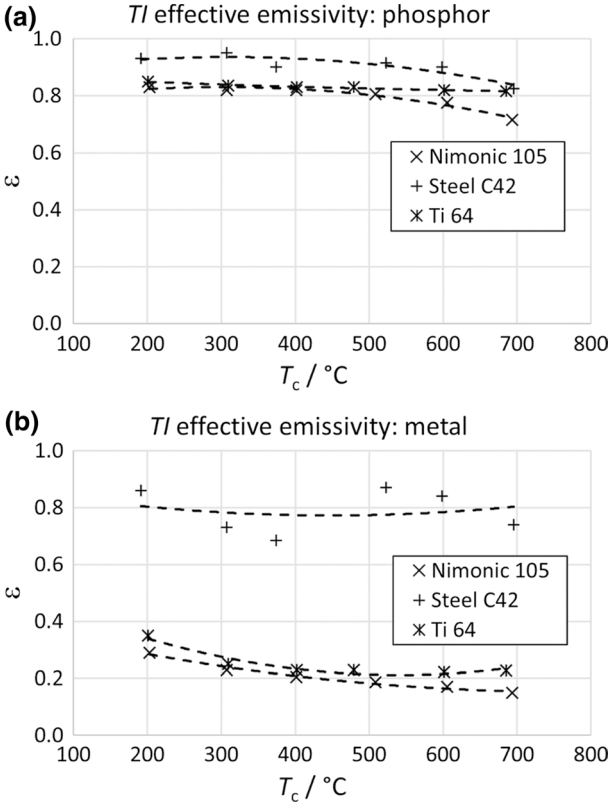

Fig. 10 The thermal imager emissivity setting required to give a surface temperature equal to that measured by the thermocouple: (a) phosphor coating and b) bare metal

strongly sample dependent and weakly temperature dependent, with mean values (averaged over all temperatures) of 0.205, 0.784 and 0.252 for *Nimonic 105*, *C42 MOD steel* and *Ti64* respectively.

Figure 11 shows photographs of two of the samples following heat treatment. In a) the *Nimonic 105* sample with visible evidence of minor oxidation is shown. In b) the *C42 MOD steel* sample with visible evidence of major oxidation is shown. These photographs support the apparent low and high surface emissivities, respectively, presented in Fig. 10b). It is also worthy of note that the effective emissivities of the phosphor coatings (Fig. 10a)) appear to be ranked in magnitude with those of the bare metals (Fig. 10b)) on which they are coated. This may simply be a coincidence, but previous experiments have shown that the phosphor coatings are translucent (at visible wavelengths, at least), which may suggest that the metal substrate does contribute to the coating's effective emissivity.

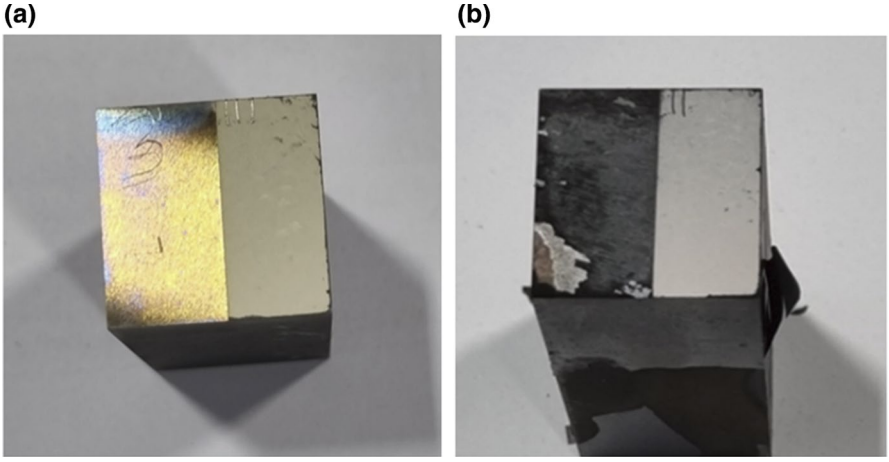

Fig. 11 Samples following heat treatment at up to 700 °C: Example of (a) low emissivity metal—*Nimonic 105* (little oxidation) and (b) high emissivity metal—*C42 MOD Steel* (strong oxidation)

9 Summary and Conclusions

We have described the field trials using luminescence versus thermal imaging thermometry during heat treatment of engineering alloys up to 750 °C in an induction heating system, with the objective of using luminescence thermometry to improve the accuracy of conventional thermal imaging. A novel imaging phosphor thermometer using the intensity ratio technique, over the range 20 °C–750 °C, was developed specifically for this work, and a description of the coating, camera system, and a robust calibration method were described in detail. Seven different engineering alloy samples were prepared, three of which were used during the field trials at the AFRC. Thermal measurements within an induction heating system that benefited from the absence of background thermal radiation, were performed on each sample from 200 °C to 700 °C in 100 °C steps.

For each sample, the phosphor derived temperatures were compared with a calibrated thermocouple embedded in the sample (2 mm below the surface). The differences were less than 45 °C over the whole temperature range (200 °C to 700 °C) and less than 35 °C below 600 °C. The third sample *Ti64* was found to have the largest differences, and this was believed to be due to the fact that the sample/coating were not annealed prior to tests, unlike the other two samples, where the differences were less than 12.4 °C below 600 °C. Positive temperature differences of up to 45 °C were seen for the phosphor measurements above 600 °C that are believed to be due to signal contamination from the excitation light reflected into the signal path, when higher excitation intensities were required to generate sufficient luminescence at the highest temperatures.

Thermal imager measurements, with the instrument emissivity set to 1.0, were made on both the phosphor coating and bare metal of each sample, indicating that a) the phosphor coating gave temperature errors of less than approximately 100 °C

(reducing with temperature in all cases), and b) the bare metal gave temperature errors of as much as 500 °C at 700 °C, reducing to 200 °C at 200 °C. However, in the case of *C42 MOD steel* sample, the errors were less than 100 °C, probably due to its higher state of oxidation and higher emissivity.

Finally, the thermal imager's emissivity was adjusted until its temperature agreed with that of the thermocouple, when measuring on first the phosphor coating and then the bare metal. In the case of the phosphor coating, the effective emissivity was relatively high, ranging from 0.72 to 0.95, reducing slightly with increasing temperature. In the case of the bare metal, the effective emissivity was strongly sample dependent and weakly temperature dependent, with mean values (averaged over all temperatures) of 0.205, 0.784 and 0.252 for *Nimonic 105*, *C42 MOD steel* and *Ti64*, respectively.

Since the phosphor derived temperatures had smaller temperature errors than the thermal imager, it is suggested that this method can be used in future measurements to compliment the more traditional thermal imaging technique, by providing a robust mechanism for adjustment of the instrument emissivity until good agreement between the thermal imager and phosphor thermometer is obtained. In principle, the phosphor thermometer could also be used to monitor changes in the sample under tests' emissivity, as changes in the bare metal's emissivity will affect the thermal imager's measurement but not that of the luminescence thermometer. Future work should also be undertaken to better quantify the perturbation the phosphor coating has on the surface temperature as this has not been considered in any detail in this work.

Appendix 1

Lumninescence Thermometer Calibration

Introduction

The imaging luminescence thermometry system described in Sect. 2 was calibrated using Sample 5 (*Ti64*) adapted specifically for calibration purposes. Calibrated thermocouples were placed within the sample, parallel to the phosphor coated surface, at depths of 5 mm and 10 mm below it. The tips of the thermocouples were placed below the centre of the phosphor region. A 60 μm phosphor coating coved only half of the front surface. The sample was placed at the end of a small tube furnace, thermally insulated on its sides and front, apart from a 1 cm × 1 cm opening above the phosphor to allow for the imaging luminescence thermometer to measure the surface. The rear surface of the metal block was not insulated, and it is assumed that the majority of the heating is on this surface. The heat transfer is assumed to be axial (i.e. 1D) with convective and radiative heat loss from the exposed area of the front surface.

Figure 12 shows a schematic of the calibration sample, with an exploded view on the LHS and combined view on the RHS. Figure 12b) shows the view from the front, with the position of the hole in the insulation visible. Figure 12c) shows a photograph of the sample with the position of the thermocouple holes relative to the phosphor coating clearly visible.

Model

Simple 1D analytical and full COMSOL Finite element heat transfer models were developed to determine the relationship between the temperature of the two thermocouples and that of the phosphor coating surface. The thermal conductivity of the *Ti64* sample and phosphor coating were taken from literature and prior measurements at NPL, respectively. The temperature of the two thermocouples can be used to estimate that of the metal surface via extrapolation. The models can then be used to determine the difference between this temperature and that of the phosphor surface. By doing this, a reasonable estimate of the true surface temperature can be obtained from the two thermocouple measurements, and a robust calibration can be obtained for the phosphor coating (i.e. intensity ratio versus temperature).

Both models require estimations of the phosphor coating thickness t_{phos}, surface emissivity ϵ and convective heat transfer coefficient h_{conv}. The coating thickness was measured with an inductive thickness gauge to be between 50 µm and 100 µm

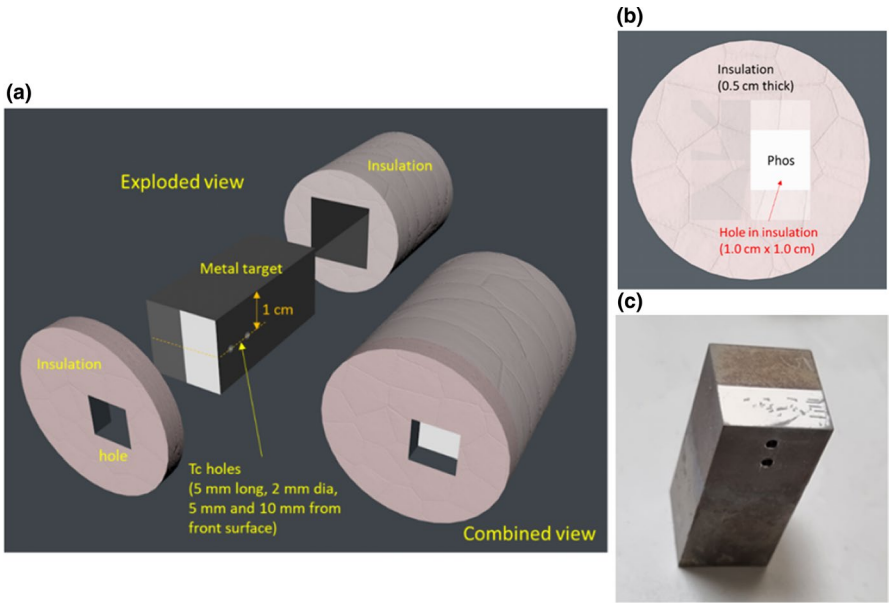

Fig. 12 Schematic of the calibration target: (a) Perspective—exploded view (LHS), combined view (RHS), (b) Front—showing position of the hole in the insulation, (c) photograph of the sample showing the position of the thermocouple holes relative to the phosphor coating

Table 1 Parameters chosen for the thermal models

Parameter	Best case	Worst case
ε	0.5	1.0
h_{conv}/ W.m^{-2}.K^{-1}	2.5	25
t_{phos}/ µm	50	100

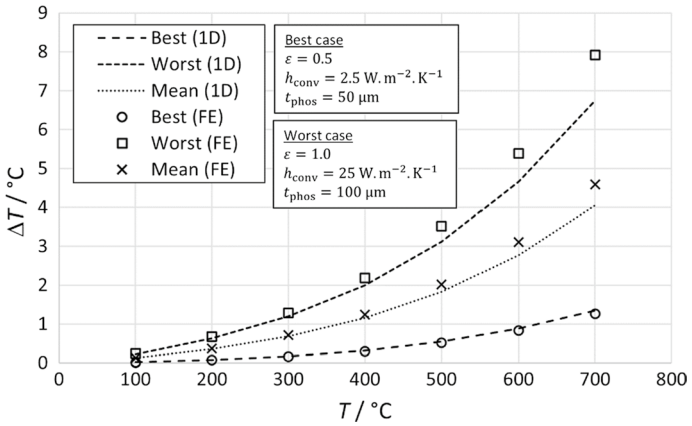

Fig. 13 Comparison of thermal models: error in the inferred phosphor surface temperature due to the coating

(60 µm average). However, ε and h_{conv} are unknown. To deal with this uncertainty, we assume a best and worst case scenario that give the smallest and largest temperature differences across the coating. These are shown in Table 1.

Figure 13 shows the results of the two models: 1D is for the simple 1D analytical model, and FE is for the full 3D Finite element model. We see that agreement between the two models is excellent and that differences between the temperature of the metal surface determined from the thermocouple extrapolation and that of the phosphor can be as large as 8 °C in the worst case scenario at 700 °C. To obtain the true surface temperature, we chose to subtract the mean error shown in the figure from our extrapolation and assume an uncertainty in the correction equal to the difference between the worst and best cases divided by two.

Measurements

With Sample 5 (*Ti64*) installed in the end of the small single zone furnace, instrumented with two calibrated Type-N thermocouples (1 mm diameter, mineral insulated, with steel sheaths), and insulated with super-wool as shown in Fig. 12, the furnace was heated up to approximately 1000 °C, resulting in an extrapolated surface temperature of approximately 740 °C.

The luminescence thermometer was configured to measure the mean intensity ratio of an (8 mm x 8 mm) square region of the exposed phosphor sample (Fig. 12b))

and simultaneously measure the two embedded thermocouples. The furnace set-point was then gradually reduced over an 8 h period and measurements of intensity ratio and the thermocouple temperatures made.

Above 500 °C, both the excitation strength $\left(V_{\mathrm{exc}}\right)$ and the exposure time (*Exp*) of the luminescence thermometer were decreased regularly to maintain a strong luminescence from the phosphor coating but avoid camera over-exposure—the luminescence of the coating increased strongly as the sample cooled from 740 °C to 500 °C. Below 500 °C, no changes in either instrument parameter were required.

Once the furnace had cooled down to ambient temperatures (approximately 20 °C), the collected data were extracted and processed to generate the calibration curve, noting that the mean temperature errors shown in Fig. 13 were subtracted from the extrapolated surface temperatures determined from the two thermocouple measurements.

Results

Figure 14 shows a) the calibration data and b) the relative sensitivity (%/°C) for the system—the sensitivity decreases with increasing temperature, with a minima around 450 °C, then increases to a maxima around 650 °C, before reducing to close to zero at around 750 °C.

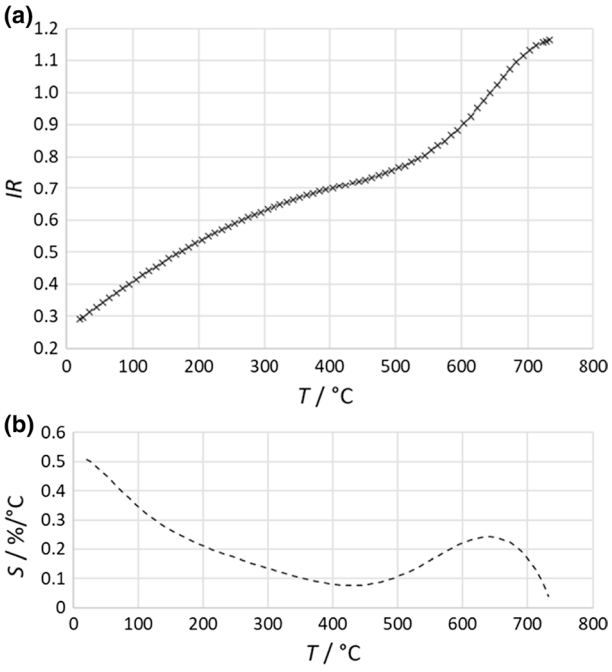

Fig. 14 Luminescence thermometer calibration: (a) *IR* and (b) *Relative sensitivity S* (%/°C), versus *T*

The calibration data were then loaded into the instrument software, so that subsequent measurements could report true surface temperatures directly.

Repeatability and luminescence strength

Figure 15 shows the reproducibility of the luminescence thermometer calibration with subsequent heat-up cycles. The differences from the initial calibration (heat-up cycle 1) are shown. Apart from some minor structure in the differences from 400 °C to 500 °C, there is no strong evidence of any drift in the system (coating/instrument). This suggests that the *MFG*/IP coating has remained stable and adhered to the calibration sample for all tests.

The strength of the luminescence as measured by the camera system depends on many factors—temperature; coating thickness, composition and structure; excitation strength V_{exc} and camera exposure time *Exp*. During tests, both V_{exc} and *Exp* were adjusted to maximise signal to noise levels but assume that all coating related phenomena remain unchanged and, at the very least that the intensity ratio versus temperature remains consistent (Fig. 15 shows this to be the case).

To examine this further, we make use of the recorded parameters $I_{\mathrm{max}}(635)$ and $I_{\mathrm{max}}(660)$, the maximum intensity (pixel count) found over the whole image once the background light has been subtracted at 635 nm and 660 nm, respectively. These parameters may be perturbed by bright parts of the image that are not used in the measurement area, so they may contain errors and should be used with caution. In Fig. 16 we plot $I_{\mathrm{max}}(635)/\left(V_{\mathrm{exc}} \cdot Exp\right)$ and $I_{\mathrm{max}}(660)/\left(V_{\mathrm{exc}} \cdot Exp\right)$, to remove the excitation strength and camera exposure dependences on the apparent emission strength.

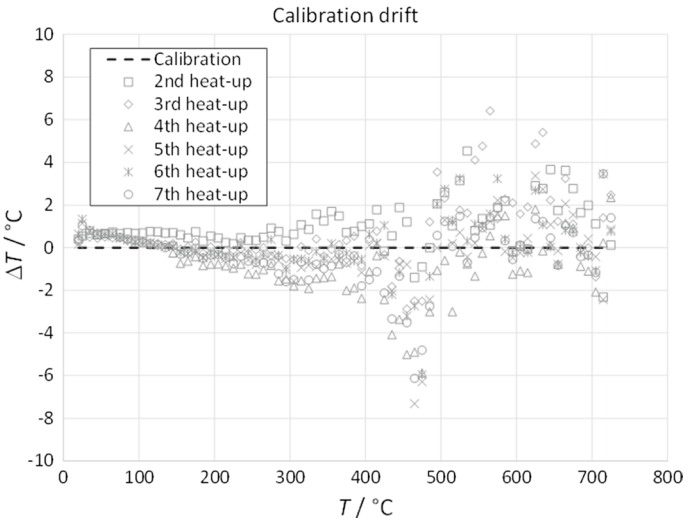

Fig. 15 Luminescence thermometer calibration drift versus thermal cycle

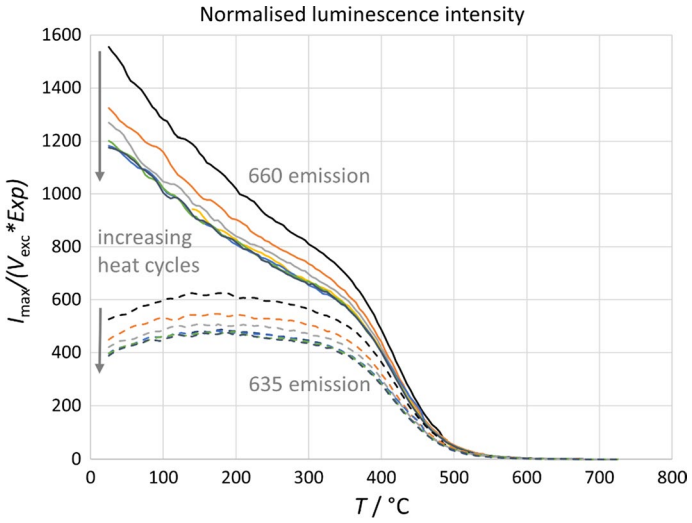

Fig. 16 Change in normalised luminescence intensity versus temperature for all thermal cycles

We see that the apparent luminescence falls with: a) increasing temperature, with a distinct reduction between 350 °C and 500°—this reduction is as expected as the phosphor exceeds it *quenching temperature* around 400 °C; and b) heat-up cycle number, at least for the first 4 cycles. However, the intensity ratio does not show this behaviour, i.e. the reduction in luminescence must be proportionate at both wavelengths.

We examine the reduction in luminescence in more detail in Fig. 17, where the percentage change in the luminescence is plotted versus heat-up cycle for all temperatures up to 400 °C. The largest reduction is between the first (calibration) and second heat-up cycles, amounting to between 10 and 15% depending

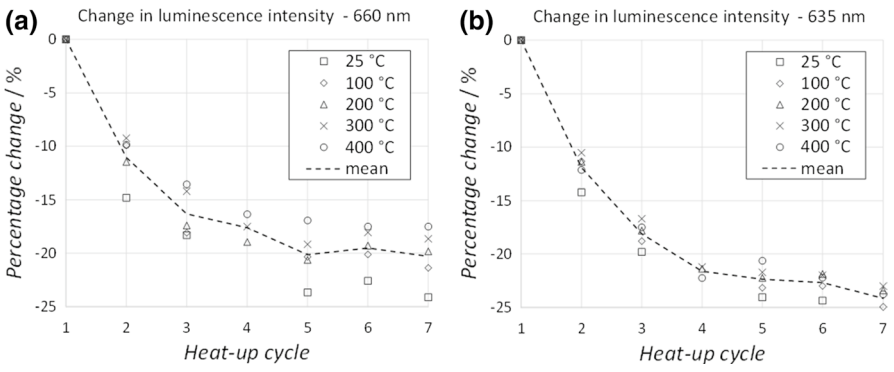

Fig. 17 Change in normalised luminescence intensity versus thermal cycle for temperatures up to 400 °C

on temperature. There are smaller reductions with subsequent heat-up cycles ultimately resulting in changes of up to 25% when all tests are considered.

The reduction in luminescence with thermal cycle is similar at both measurement wavelengths, explaining why the calibration appears to remain unchanged, e.g. no signs of systematic drift in Fig. 15.

It is also worthy of note that the reduction in luminescence appears to stabilise by the $5^{th}/6^{th}$ cycle suggesting that the coating will provide reliable temperature measurements for extended periods of time.

Uncertainty budget

To determine the uncertainty budget for the imaging luminescence thermometer calibration, we follow the ISO guide *Evaluation of measurement data—guide to the expression of uncertainty in measurement* [21]. The purpose of the calibration is to determine the functional relationship between the measured luminescence temperature T_{phos} and the independent calibration quantities X_i. This can be expressed as:

$$T_{\text{phos}} = f\left(X_i\right) \tag{8}$$

The combined standard uncertainty of such a measurement can be written as:

$$u_{\text{c}}\left(T_{\text{phos}}\right) = \sqrt{\sum_{i=1}^{N} \left(\frac{\partial f}{\partial x_i}\right)^2 u^2\left(x_i\right)} \tag{9}$$

where x_i is the estimate of X_i, $u\left(x_i\right)$ is the standard uncertainty of this estimate and $\partial f / \partial x_i$ is the partial derivative of f with respect to x_i, commonly called the sensitivity coefficient. For our analysis, we present all standard uncertainties in terms of temperatures. This results in $\partial f / \partial x_i = 1$ for all i, leading to the expression:

$$u_{\text{c}}\left(T_{\text{phos}}\right) = \sqrt{\sum_{i=1}^{N} u^2\left(x_i\right)} \tag{10}$$

The calibration quantities x_i, which are specific to the phosphor/binder combination, are as follows:

U1 *Measurement standard deviation*—this is the maximum standard deviation of the measured phosphor temperature over the calibration temperature range (20 °C to 750 °C), taken from the mean intensity ratio of an (8 mm x 8 mm) square region of the exposed phosphor sample.

U2 *ITS-90 thermocouple calibration*—the two thermocouples were traceably calibrated in a dry-block facility prior to installation in the calibration target.

U3 *Surface temperature extrapolation*—this accounts for the uncertainty introduced in determining the surface temperature of the phosphor coating using the model

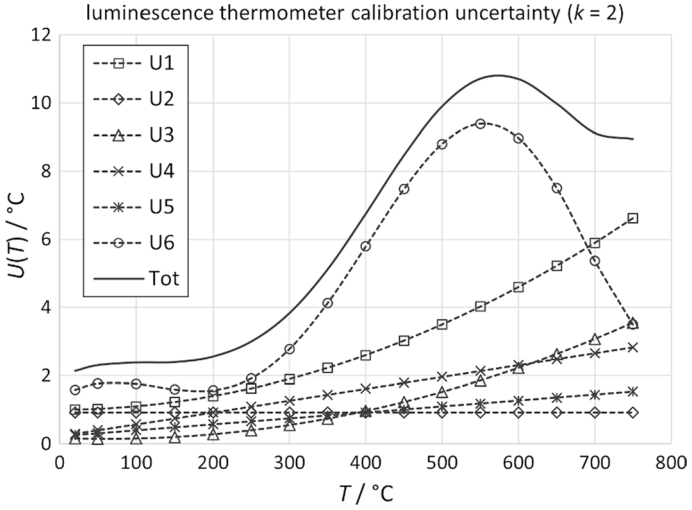

Fig. 18 Calibration uncertainty budget for the imaging intensity ratio luminescence thermometer. The uncertainty components are calculated for a coverage factor of k = 2 (95% confidence interval)

shown in Fig. 13. An uncertainty in the correction equal to the difference between the worst and best cases divided by two is used.

U4 *Coating thickness*—this accounts for variation in the phosphor coating thickness over the measurement region and its effect on the measured intensity ratio.

U5 *Phosphor heating due to LED*—this acounts for the small temperature rise that occurs due to absorption of the excitation light.

U6 *Thermal cycling drift*—this component was determined from the calibration drift shown in Fig. 15 with repeated thermal cycling. This is the largest component of uncertainty in the calibration uncertainty budget.

In accordance with Eq. 10, i.e. combining the individual components of uncertainty in quadrature, the calibration uncertainty budget is presented in Fig. 15, where an expanded uncertainty with a coverage factor of $k=2$ (95% confidence interval) is shown. The standard calibration uncertainty is below 3 °C at 20 °C, rising to approximately 11 °C for temperatures around 600 °C and above (Fig. 18).

Appendix 2: Tabulated results

See Tables 2, 3, and 4.

Table 2 Sample 3, Nimonic 105

T_{phos} / °C	T_c / °C	TI(phos, $\varepsilon=1$) / °C	TI(met, $\varepsilon=1$) / °C	ε(metal)	ε(phos)	T_{phos}-T_c / °C	ΔTI(phos) / °C	ΔTI(metal) / °C
197	202.8	171	–	0.290	0.830	− 5.6	− 31.8	− 202.8
298	307.4	262	–	0.230	0.820	− 9.4	− 45.4	− 307.4
389	401.4	341	124	0.205	0.820	− 12.4	− 60.4	− 277.4
500	508.6	432	156	0.187	0.805	− 8.6	− 76.6	− 352.6
609	605.5	514	183	0.170	0.775	3.5	− 91.5	− 423.0
735	693.2	586	205	0.150	0.715	41.8	− 107.2	− 488.2

Table 3 Sample 2, *C42 MOD steel*

T_{phos} / °C	T_c / °C	TI(phos, $\varepsilon=1$) / °C	TI(met, $\varepsilon=1$) / °C	ε(metal)	ε(phos)	T_{phos}-T_c / °C	ΔTI(phos) / °C	ΔTI(metal) / °C
188	191.4	177	168	0.860	0.930	− 3.4	− 14.4	− 23.4
300	307.5	281	246	0.730	0.950	− 7.5	− 26.5	− 61.5
368	374.0	346	286	0.685	0.900	− 6.0	− 28.0	− 88.0
512	523.0	484	467	0.870	0.915	− 11.0	− 39.0	− 56.0
590	598.7	551	526	0.840	0.900	− 8.7	− 47.7	− 72.7
723	695.3	635	591	0.740	0.825	27.7	− 60.3	− 104.3
575	586.5	539	493	0.790	0.905	− 11.5	Repeat measurements	
370	378.0	350	306	0.760	0.920	− 8.0		

Table 4 Sample 6, *Ti64*

T_{phos} / °C	T_c / °C	TI(phos, $\varepsilon=1$) / °C	TI(met, $\varepsilon=1$) / °C	ε(metal)	ε(phos)	T_{phos}-T_c / °C	ΔTI(phos) / °C	ΔTI(metal) / °C
198	200.6	174	–	0.350	0.850	− 2.6	− 26.6	− 200.6
283	309.0	272	108	0.250	0.835	− 26.0	− 37.0	− 201.0
367	402.0	355	142	0.230	0.830	− 35.0	− 47.0	− 260.2
457	479.0	423	175	0.230	0.830	− 22.0	− 56.0	− 304.0
605	601.5	526	218	0.222	0.820	3.5	− 75.5	− 383.5
729	685.2	599	254	0.228	0.815	43.8	− 86.2	− 431.2

Acknowledgements The authors would like to thank Laura Bevilacqua for preliminary investigative work on the phosphor coated alloy samples and Dave Lowe for technical review of the manuscript.

Funding This project has received funding from the EMPIR programme co-financed by the Participating States and from the European Union's Horizon 2020 research and innovation programme (Grant Number 17IND04). In part, this work was funded by the UK Government's Department for Business, Energy and Industrial Strategy (BEIS) through the UK's National Measurement System programmes.

References

1. J.V. Pearce, F. Edler, C.J. Elliott, L. Rosso, G. Sutton, S. MacKenzie, G. Machin, *EMPRESS—A European Project to enhance process efficiency through improved temperature measurement*, , Proc. 17th International Congress of Metrologie (2015), EDP Sciences. https://doi.org/10.1051/metrology/20150008001 (2015).
2. Euramet project *EMPRESS2*, https://www.euramet.org/research-innovation/search-research-projects/details/project/enhancing-process-efficiency-through-improved-temperature-measurement-2/
3. J.V. Pearce, EMPRESS: a pan-European project to enhance manufacturing process efficiency through improved temperature control. Meas. Control **49**(8), 252–255 (2016)
4. Z.M. Zhang, G. Machin, Experimental methods in the physical. Sciences **42**, 1–28 (2009). https://doi.org/10.1016/S1079-4042(09)04201-5
5. G.D. Nutter, D.P. DeWitt, Theory and Practice of Radiation Thermometry, Wiley-Interscience (1989), ISBN-13: 978–0471610182.
6. L. Michalski, K. Eckersdorf, J. Kucharski, J. McGhee, *Temperature Measurement* (Wiley, New York, 2001), pp. 403–404. ISBN 978-0-471-86779-1.
7. R. Corwin, A. Rodenburgh, Temperature error in radiation thermometry caused by emissivity and reflectance measurement error. Appl. Opt. **33**, 1950–1957 (1994). https://doi.org/10.1364/AO.33.001950
8. J.A. Gatowski, M.K. Smith, A.C. Alkidas, An experimental investigation of surface thermometry and heat flux. Exp. Therm. Fluid Sci. **2**(3), pp. 280–292, ISSN 0894-1777 (1989). https://doi.org/10.1016/0894-1777(89)90017-4.
9. J. Brübach, C. Pflitsch, A. Dreizler, B. Atakan, On surface temperature measurements with thermographic phosphors: a review. Prog. Energy Combust. Sci. **39**, 37–60, ISSN 0360-1285, https://doi.org/10.1016/j.pecs.2012.06.001. (2013)
10. A.H. Khalid, K. Kontis, Thermographic phosphors for high temperature measurements: principles, current state of the art and recent applications. Sensors **8**, 5673–5744 (2008). https://doi.org/10.3390/s8095673
11. M. Aldén et al., Thermographic phosphors for thermometry: a survey of combustion applications. Prog. Energy Combust. Sci. **37**, 422–461 (2011)
12. G. Sutton et al., Imaging phosphor thermometry from T = 20 °C to 450 °C using the time-domain intensity ratio technique. Meas. Sci. Technol. **30**, 044002 (2019). https://doi.org/10.1088/1361-6501/ab04ea
13. *Indestructible Paints Ltd*, 16 25 Pentos Drive, Sparkhill, Birmingham, B11 3TA.
14. *Magnesium-fluorogermanate phosphor (Mg_4FGeO_6:Mn)*, Phosphor SV 067 N, OSRAM GmbH.
15. *Thorlabs Inc* (www.thorlabs.com).
16. *Prizmatix*, POB 244, Givat-Shmuel 5410102, Israel.
17. *National Instruments*, 11500 N Mopac Expwy, Austin, TX 78759–3504.
18. https://www.ametek-land.com/products/ir-thermal-imagers-and-line-scanners/arc-radiometric-thermal-imager
19. Certificate of calibration 24668, ARC 8/22/1000 HF, ID number 197160 32, 25 September 2020.
20. *Sauter TC 1250-0.1 F* Thickness Gauge, https://uk.rs-online.com/web/p/thickness-gauges/6608133/
21. BIPM, *Evaluation of measurement data - Guide to the expression of uncertainty in measurement*, JCGM 100:2008